Paper No.
00000 (Official use)

CORCON 2019
Mumbai, India.
23rd - 26th September

Breakthrough in Pulsed Eddy Current Detection and Sizing

Charles Tremblay[1], **Marco Michele Sisto**[1], **Andréanne Potvin**[1]
[1]Eddyfi Technologies, Québec, Canada

ctremblay@eddyfi.com

ABSTRACT

Pulsed Eddy Current (PEC) has been successfully deployed over the last decades for a variety of corrosion-related applications, especially for the inspection of Corrosion Under Insulation (CUI) inspections, Corrosion Under Fireproofing (CUF), Flow-Accelerated Corrosion (FAC) and offshore assets corrosion. This technology has proven to be an efficient screening tool, allowing for the detection of corrosion without having to remove coating or insulating material over typical pipes, tanks and vessels. While being very well adapted to these oil and gas-related applications where the insulation is thick and in which the damage mechanisms result in quite generalized corrosion, up to now, it has never been specifically developed for some of the most important naval and offshore applications. Ship floors and corrosion scabs on pipelines for instance, are applications in which a PEC probe can be brought much closer to the inspected steel but in which the corrosion damage is more localized and therefore, more difficult to detect and size with the previously available technologies. Here, we are presenting a new ensemble of products resulting from intensive research and development efforts aimed at achieving better defect detection and sizing performances in low lift off conditions. The new solution involves an innovative sensor design and the required adapted sizing algorithms as well as new and unique analysis tools to help increase the analyst's confidence level in the reported indications. The new technological breakthroughs will be discussed. Application examples with context and results will be provided.

Keywords: *pulsed eddy currents, array probes, NDT, corrosion under insulation, corrosion under fireproofing, marine, naval and offshore corrosion*

1 INTRODUCTION

Pulsed Eddy Current (PEC) has been successfully deployed over the last decades for a variety of corrosion-related applications, especially for the inspection of Corrosion Under Insulation (CUI) inspections, Corrosion Under Fireproofing (CUF), Flow-Accelerated Corrosion (FAC) and offshore assets corrosion. This technology has proven to be an efficient screening tool, allowing for the detection of corrosion without having to remove coating or insulating material over typical pipes, tanks and vessels. While being very well adapted to these oil and gas-related applications where the insulation is thick and in which the damage mechanisms result in quite generalized corrosion, up to now, it has never been specifically developed for some of the most important naval and offshore applications. Ship floors (Figure

1) and corrosion scabs on pipelines (Figure 2) for instance, are applications in which a PEC probe can be brought much closer to the inspected steel but in which the corrosion damage is more localized or embedded in larger corroded areas, and therefore, more difficult to detect and size with the previously available technologies.

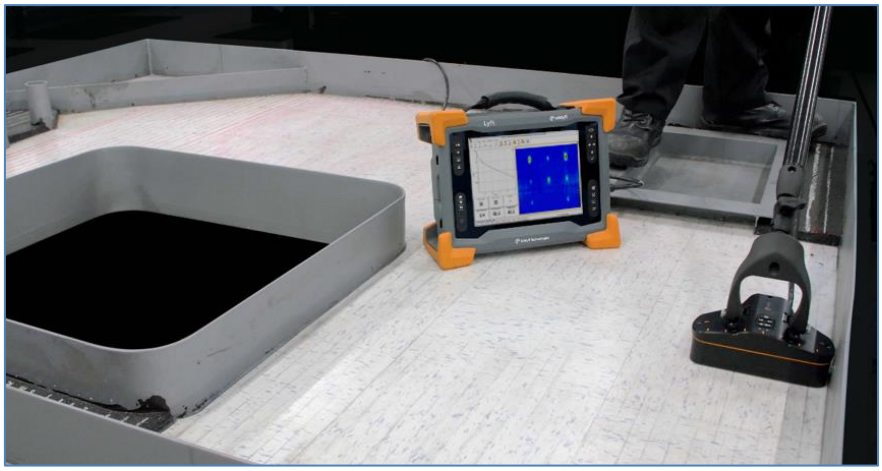

Figure 1. Application of a PEC array probe to the inspection of ship floors

Figure 2. Corrosion scabs are typical of offshore piping systems

In this paper, we are presenting two major technical breakthroughs resulting from intensive research and development efforts aimed at achieving better defect detection and sizing performances in low lift off conditions. In later sections, a new and innovative sensor design will be unveiled. Its working principle will be summarized, its performance will be detailed and application examples will be shown. To complete the picture, a new and unique analysis tool that will help increase the analyst's confidence level in the reported indications will also be presented. Its potential uses and application examples will also be provided.

2 New sensor

Past developments in PEC technology enabled more accurate sizing of small corrosion spots. Those solutions relied solely on post-processing and defect detection, among other factors, is a prerequisite for using it. In some applications where smaller corrosion spots are

embedded in generalized corrosion, such post-processing tools are inapplicable and a physical solution is required. To better understand how PEC can be improved to work in such conditions, it is important to know about one fundamental technical characteristic of PEC: the Footprint, or FP in short. As depicted in figure 3, the PEC probe footprint marks an area around the center of the probe where the sensitivity is optimal. It can be approximated using Equation 1.

$$FP \approx 0.65xLO+FP_0 \qquad \text{Eq. (1)}$$

Where LO is the Lift Off, or coating thickness, FP_0 is the footprint of the probe without lift off.

The PEC footprint is relatively large compared with, for instance, a UT spot check. The main advantage of this is that large areas are measured per single acquired data points, making the full coverage inspection of a component quite fast. However, PEC measures the average wall thickness over an area proportional to the FP, making small flaws more difficult to detect and size accurately.

These characteristics work in favor of the conditions prevalent in the petrochemical industry because for most of the related applications, high productivity is mandatory while simple detection of generalized corrosion is often good enough.

In the cases where it matters to better size the remaining ligament of a corrosion complex, or when it is wished to detect small corrosion spots embedded in larger corroded areas, a smaller footprint is required.

Past attempts of reducing the PEC footprint involved solutions based on the magnetic focusing concept. This concept relies on two concentric coils wounded in opposition to try focusing the magnetic fields onto a smaller area of the inspected area (see for example patent US8704513B2). There is hardly evidence that this concept performs well enough and having two coils working in opposition certainly cancels a big part of the magnetic energy, resulting in lesser lift off and wall thickness operating ranges.

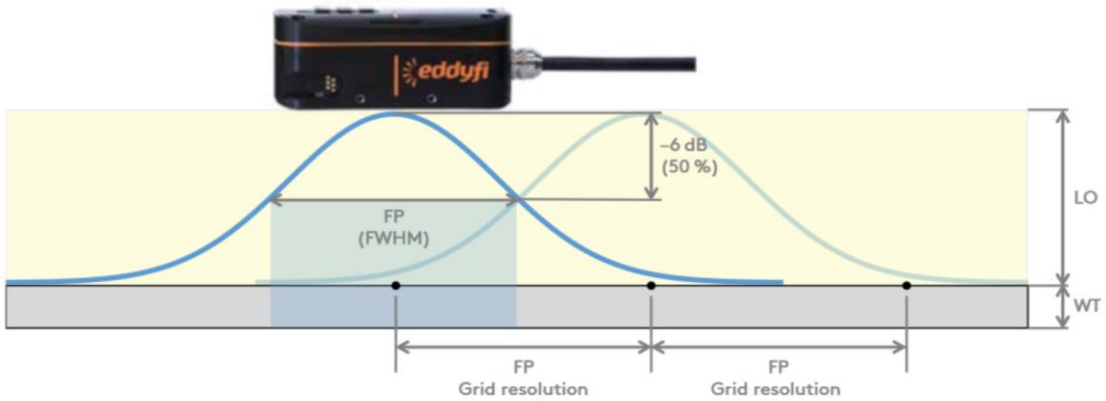

Figure 3. The PEC probe's footprint is an essential parameter of PEC. It is defined as the full width at the half maximum of the probe sensitivity bell.

High demands from the industry for PEC technology that provides detection of smaller flaws and better sizing of remaining ligaments while retaining a good application range and high productivity motivated the design of a new generation of sensors featuring deep innovations. This new sensor now exists, and in this paper, we will refer to it as the HR sensor.

2.1 Working principle

The new patent pending sensor's working principle relies on an array of dual sensors arranged in a very specific configuration and working in conjunction with a specifically designed algorithm. This system enables spatial triangulation which reduces the effective footprint of the sensor. As demonstrated in the next section, this is all achieved while retaining a very useable application range.

2.2 Performances

The performance demonstration of the HR sensor is put forward in relation with the previously available PEC sensor with the smallest footprint: The PEC-025-G2 sensor that we'll name the "G2" sensor in this paper for simplification purposes. Table 1 shows the G2 sensor application range in green; note that the HR sensor application range is the exact same.

		Insulation / Coating thickness									
		0.00 mm 0.000 in	6.35 mm 0.250 in	12.70 mm 0.500 in	19.05 mm 0.750 in	25.40 mm 1.000 in	38.10 mm 1.500 in	50.80 mm 2.000 in	63.50 mm 2.500 in	76.20 mm 3.000 in	88.90 mm 3.500 in
Wall Thickness	3.18 mm 0.125 in										
	6.35 mm 0.250 in										
	9.53 mm 0.375 in										
	12.70 mm 0.500 in										
	15.88 mm 0.625 in										
	19.05 mm 0.750 in										
	25.40 mm 1.000 in										

Table 1: Application range of the small G2 sensor and the HR sensor. The range is defined as a function of the component wall thickness and lift off, or coating thickness. The probe application range is highlighted in green.

2.2.1 Sizing performance

Figure 4 shows the comparative results between the G2 and HR sensors on small round bottom holes. The reference plate that was used has a nominal wall thickness of 6.35 mm and the studied flaws are as specified in Table 2.

Flaw ID	OD (mm)	OD (In)	Aspect ratio	Remaining wall %
1	10.2	0.40	2:1	20%
2	20.6	0.81	5:1	35%
3	8.3	0.33	2:1	35%

Table 2: Specifications of the flaws used in a comparative study of the sizing performance between the G2 and the HR sensor.

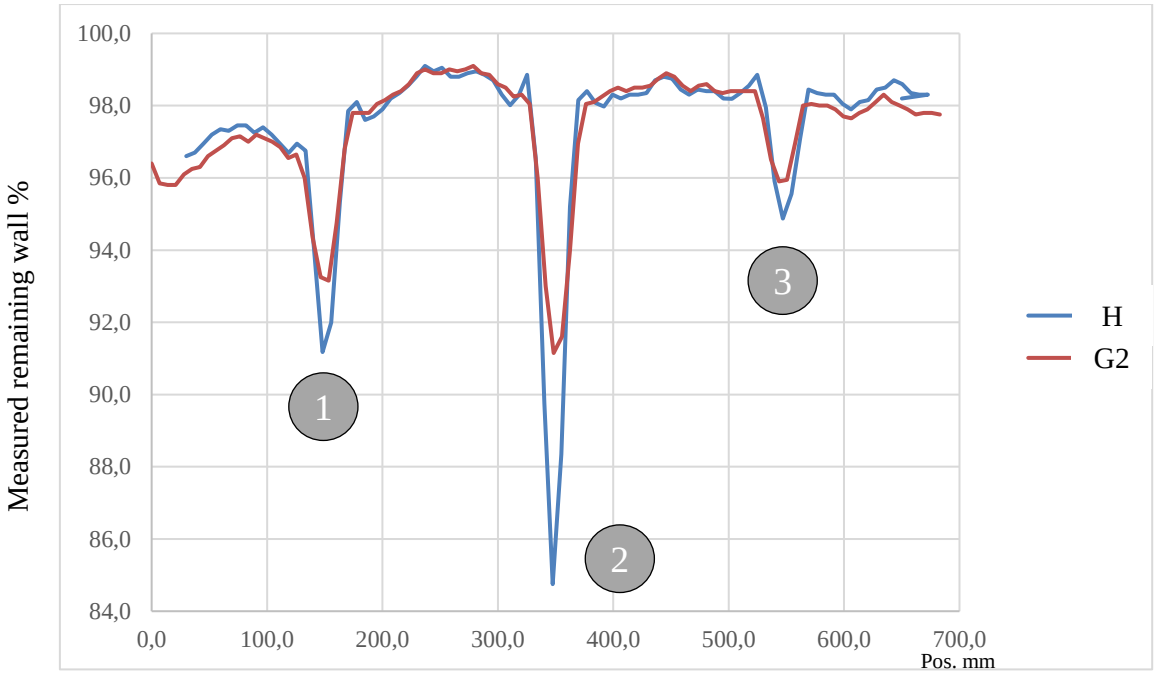

Figure 4. Comparison between the measurement of small flaws using the G2 sensor in brown and the HR sensor in blue.

Detailed results are tabulated in Table 3.

	Flaw 1	Flaw 2	Flaw 3
G2 sensor measured wall thickness %	93.3	91.2	96
HR sensor measured wall thickness %	91.2	84.8	94.9
Accuracy improvement %	2.1	6.4	1.1

Table 3: Comparative table between the measurements obtained using the G2 and HR sensors on the small flaws reference plate.

Notice the improvement in accuracy on the flaw measurements when going from the G2 sensor to the HR sensor.

2.2.2 Detection performance

As mentioned earlier, PEC probes with larger footprints are less likely to detect small embedded corrosion spots. It is quite common, on pipe scabs for instance, to have remaining ligaments over a small area surrounded with larger corroded areas. For a quick qualitative appreciation of the detection performance of the HR sensor in such conditions, let's consider a test plate that was designed with an embedded flaw as described in Figure 5. Figure 6 shows the comparative results between the G2 sensor on the left, and the HR sensor on the right while scanning in contact with the plate. All measurements are without post-processing. Note that the embedded flaw is clearly detected with the HR sensor, while it's not using the G2 sensor. It is also worth noting that while using the larger footprint G2 sensor, the measurement is averaged over a wider area so the accuracy on the small flaw is quite off while the HR sensor measures quite accurately both the small embedded flaw and the surrounding flaw.

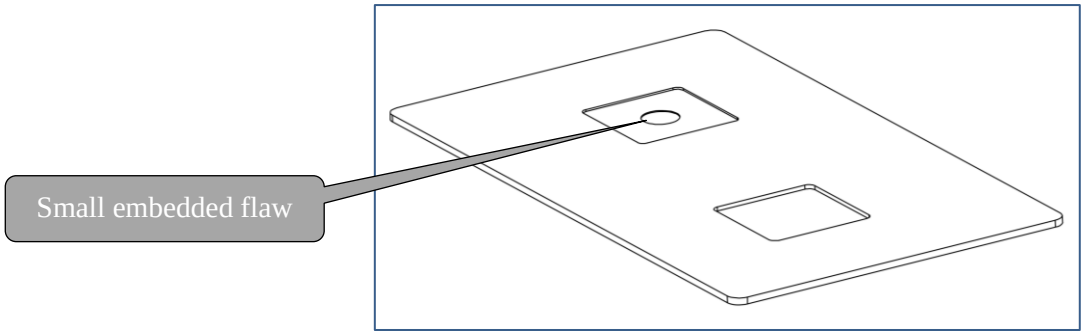

Figure 5. The reference plate used to make a comparative study for the detection of small corrosion spots embedded in larger corroded areas features a small 50% deep, 25 mm OD flaw embedded into a 30% deep, 75 mm wide square flaw.

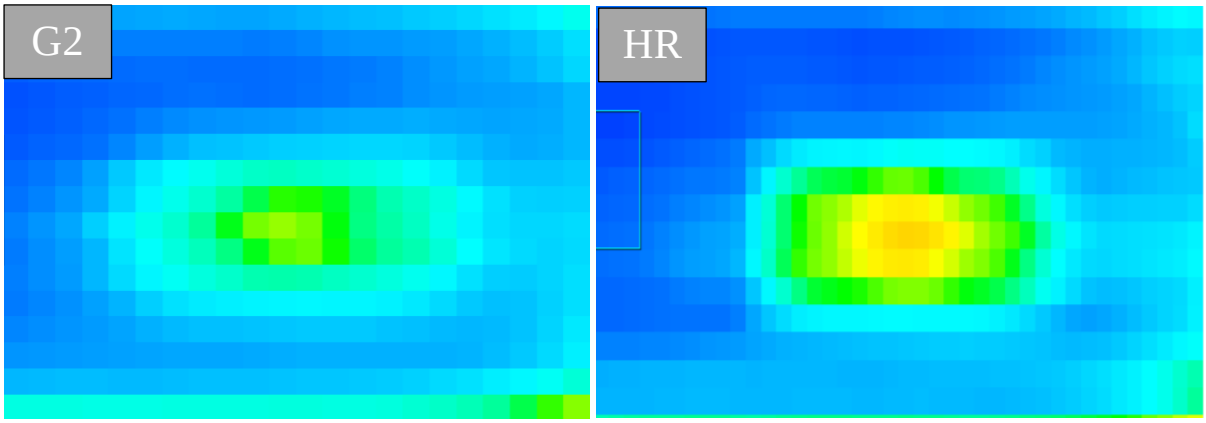

Figure 6. C-scan comparison between the small embedded flaw scanned with the G2 sensor on the left and the HR sensor on the right. The larger footprint of the G2 results in averaging with the surrounding thicker areas which results in a 20% depth undersizing while the HR sensor achieves accurate results.

To complete the picture, comparative Probability of Detection (POD) studies based on the MIL-1823A guideline were carried on and the results are presented in figure 7 in the form of a "Smallest detectable defect" chart where the smallest detectable defect volume descriptor, expressed in (defect Area)*WL%, is plotted against the probe Lift-Off (LO) in inches.

The smallest detectable defect using the HR sensor is roughly half the volume of what can be detected using a G2 sensor with equivalent application range.

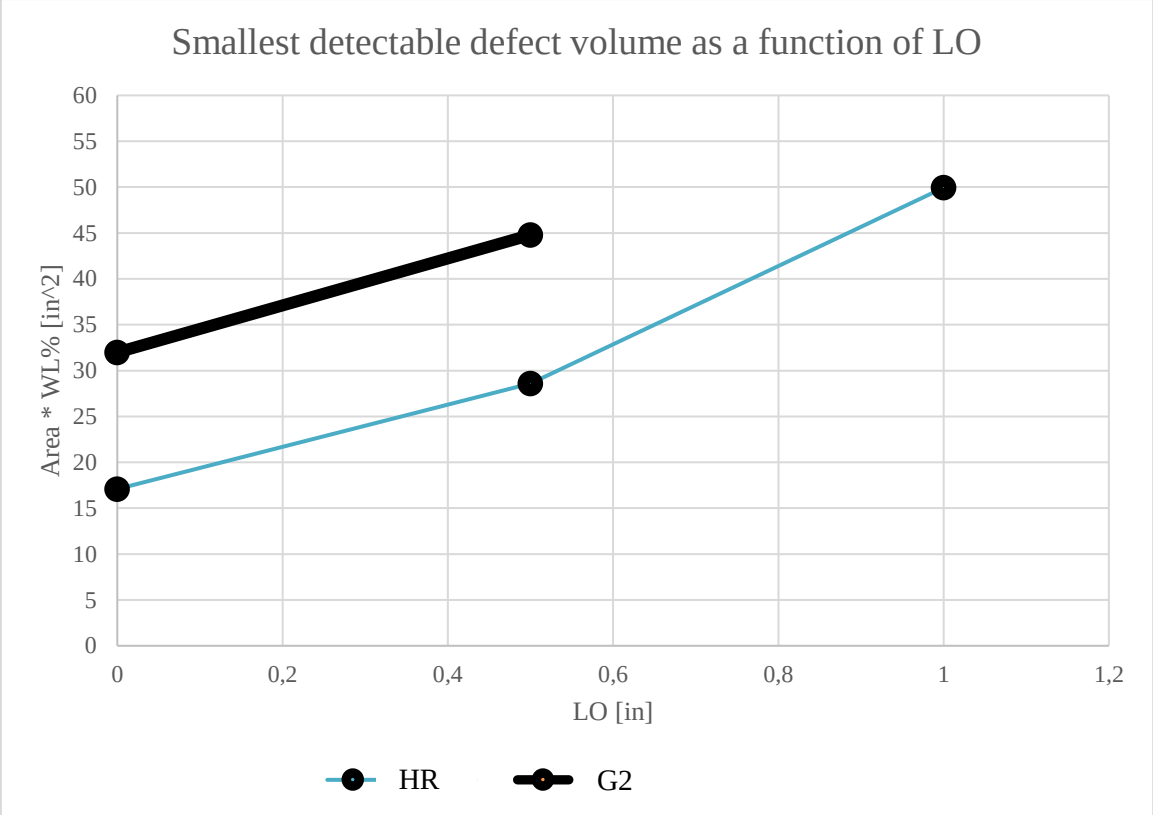

Figure 7. Smallest detectable defect chart where the smallest detectable defect volume, expressed in Area*WL%, is plotted against the probe Lift-Off (LO) in inches.

2.3 Application examples

Figure 8 shows a comparative scan of a pipe covered with scab which was decommissioned and made available to study. The pipe nominal wall thickness is 7.8 mm and features a mix of localized corrosion and more generalized corrosion.

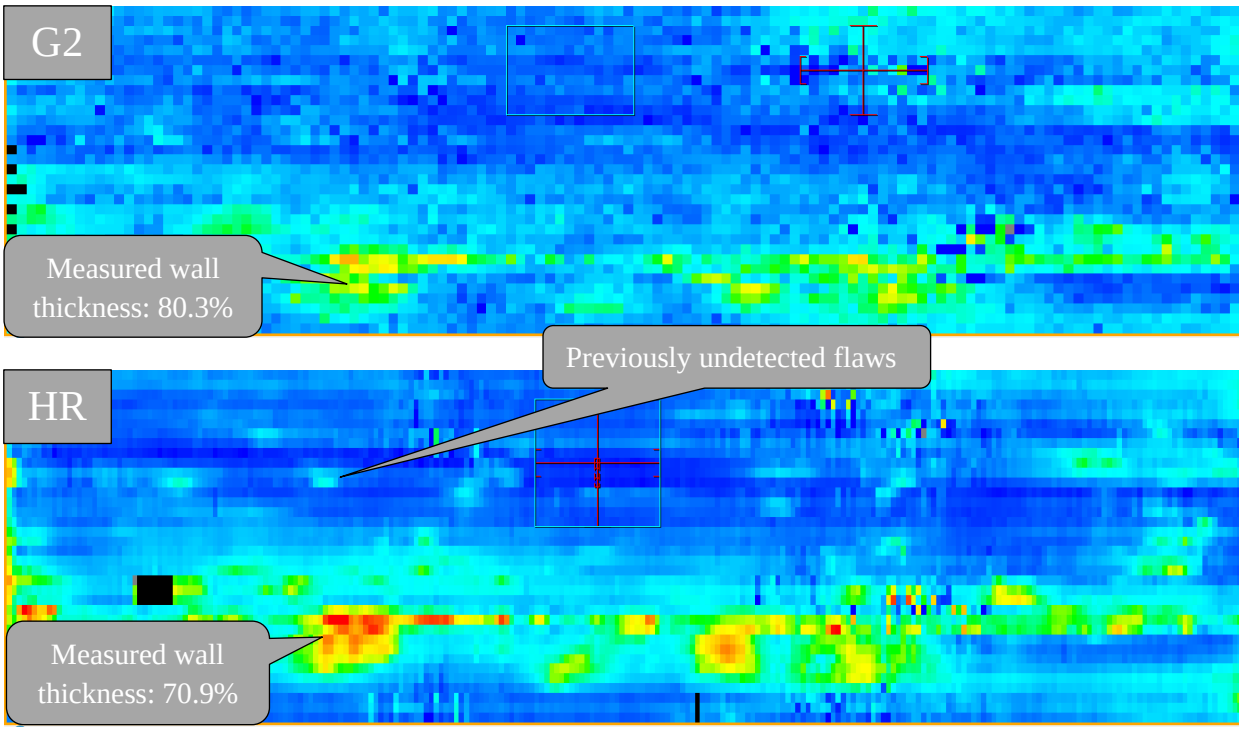

Figure 8. Comparison between the C-scans obtained using the G2 sensor above and the HR sensor below. The HR sensor enable the detection of an ensemble of previously undetected flaws and the accuracy on the deepest flaws is improved by approximately 10%.

Figure 9 shows another comparative scan of a pipe covered with three important corrosion scabs which was also decommissioned and made available to study. The pipe nominal wall thickness is 6.35 mm and features thick corrosion scabs which would be impossible to penetrate with UT for instance.

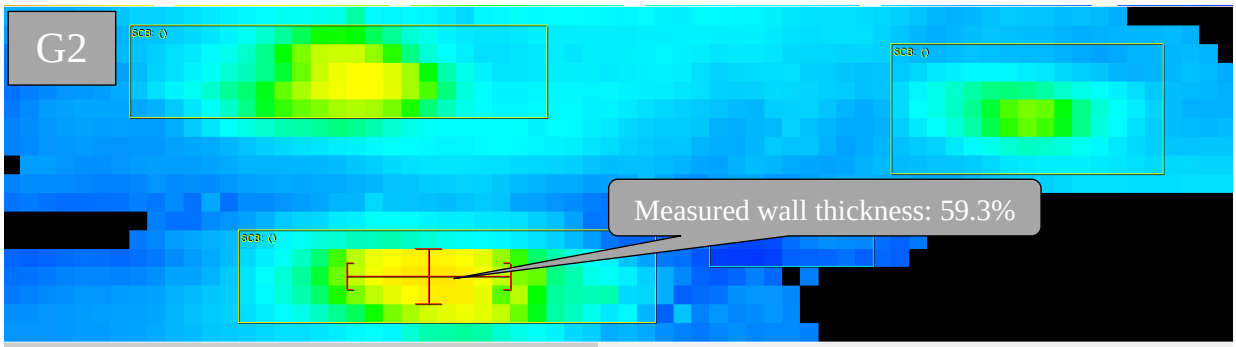

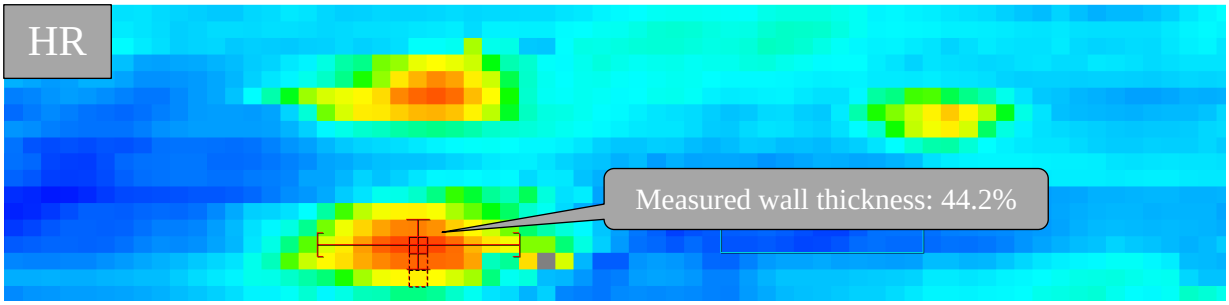

Figure 9. Comparison between the Cscans obtained using the G2 sensor above and the HR sensor below. The HR sensor achieves an accuracy roughly 15% better than the G2 sensor on the deepest flaw.

Figure 10 shows another comparative scan of a pipe covered with three important corrosion scabs which was also decommissioned and made available to study. The pipe nominal wall thickness is 6.35 mm and features one close to 25 mm thick corrosion scab which would be impossible to penetrate with UT for instance. This pipe sample was available to us since the very beginning of Eddyfi's involvement in PEC technology and was a quite interesting study subject for developments of the HR sensor because its wall thickness profile was accurately measured using UT from the ID. The minimum remaining ligament is known to be 30% wall thickness. The G2 sensor underestimates the flaw depth by about 20% while the HR sensor depth underestimation is of only 5%.

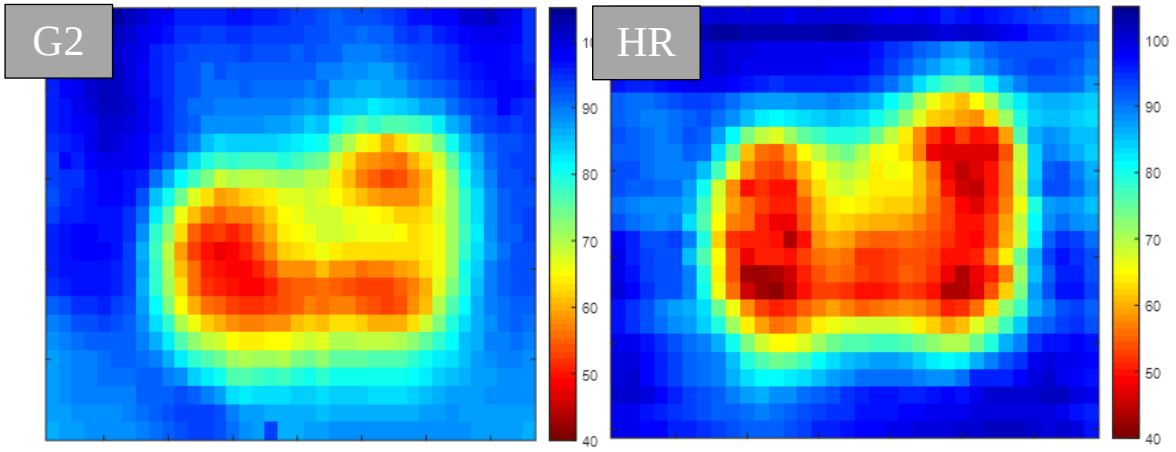

Figure 10. Comparison between the C-scans obtained using the G2 sensor on the left and the HR sensor on the right. The HR sensor achieves an accuracy roughly 15% better than the G2 sensor on the minimum remaining ligament.

3 New PEC signal analysis tool

A long-lasting plague affecting PEC technique was how difficult it is for the human eye to discern useful information from a PEC A-scan. For these reasons, for a long time the average thickness numbers were extracted using a human adjusted threshold on A-scan (Fig. log-log with threshold). The location where the A-scan would cross the subjectively adjusted threshold would correspond to an average remaining wall thickness number. Experience showed how difficult it is to accurately adjust an approximate location where a human set threshold was

defined. This, along with a couple of very simple and shallow observables constituted PEC signal analysis which made it very user dependant and not always very clear.

The user dependency was minimized a few years back with the introduction of automated setups that relies mostly on true *in situ* tests and with the introduction of a curve fit algorithm, whose development is based on an analytical model of the PEC signal. These latest developments are working well in favor of the PEC technique but still doesn't provide the inspectors with a lot to appreciate for themselves and counter verify what the clever algorithms are outputting. For instance, it's impossible for an inspector to use a PEC A-scan to clearly:

1. Estimate the remaining wall thickness
2. Distinguish small defects from large thinning areas
3. Quickly and easily identify problems in the setup configuration
4. Compare efficiently different measurements due to liftoff variations and weather jacket overlaps

Our most recent developments were directed in the creation of new analyses views and methods aimed at offering the second part of a double redundancy check that the NDT world always required.

3.1 Working principle

The idea of this new representation lies in the view of the variation rate of the log-lin (amplitude in log scale, time in linear scale) representation of the A-scan: it was therefore named the ''*Tau* curve''.

The *Tau* curve is obtained by applying equation 2 to the A-scan:

$$Tau\,[ms] = {}^{-1}\Big/\left[\frac{d}{dt} log\,(Ascan/[1V])\right] \qquad \text{Eq. (2)}$$

The main advantages of the *Tau* curve lie in the way it simplifies the main parts of the A-scan into lines and also how it eliminates the effects of lift off variations. This way, the observables are much easier to process by the human eye and the actual signal stays in close proximity to the calibration curve, making relative observations much clearer.

Figure 10 provides a comparative view between the usual log-lin A-scan and the *Tau* curve. Notice how the main parts of the curve are simplified and decomposed into two clear and distinctive lines.

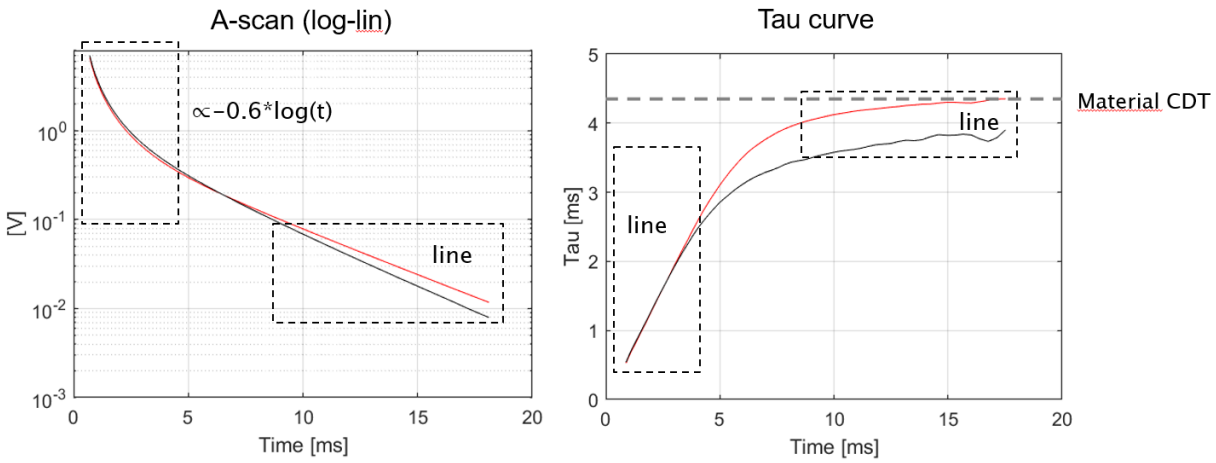

Figure 11. Comparison between two representations of the same signal. The usual A-scan in log-lin scales on the left and the *Tau* curve on the right.

Figure 11 provides a comparative view between the usual log-lin A-scan and the *Tau* curve when there is a large amplitude variation between the actual signal in black, and the calibration reference in red. Such amplitude variations, usually caused by lift off variations, makes direct A-scan comparison much more difficult. Using the *Tau* curve, the calibration reference curve and the actual measurement signal are brought back in superimposition which makes comparative analysis much easier to a human analyst.

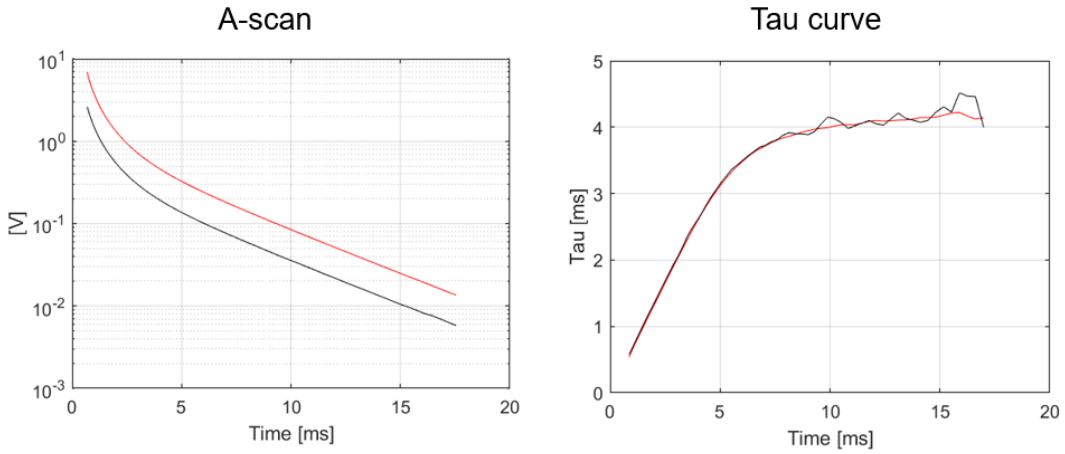

Figure 12. Comparison between two representations of the same signal in the presence of amplitude variations between the calibration reference and the actual measurement.

More details on the essential parameters of the *Tau* curve are presented in figure 12. It features two main curves and one slope marker. The red curve is from the calibration reference, the black curve is from the actual data point and the blue dotted line is a slope marker for the initial part of the signal. The initial part of the signal has a slope which happens to be characteristic of the inspected material. A slope of time/1.6 is characteristic of the low alloyed carbon steels whereas for the cast irons, it is time/1.7. The inspected material characteristic decay time, or CDT in short, can also be estimated by projecting the later line to the *Tau* axis.

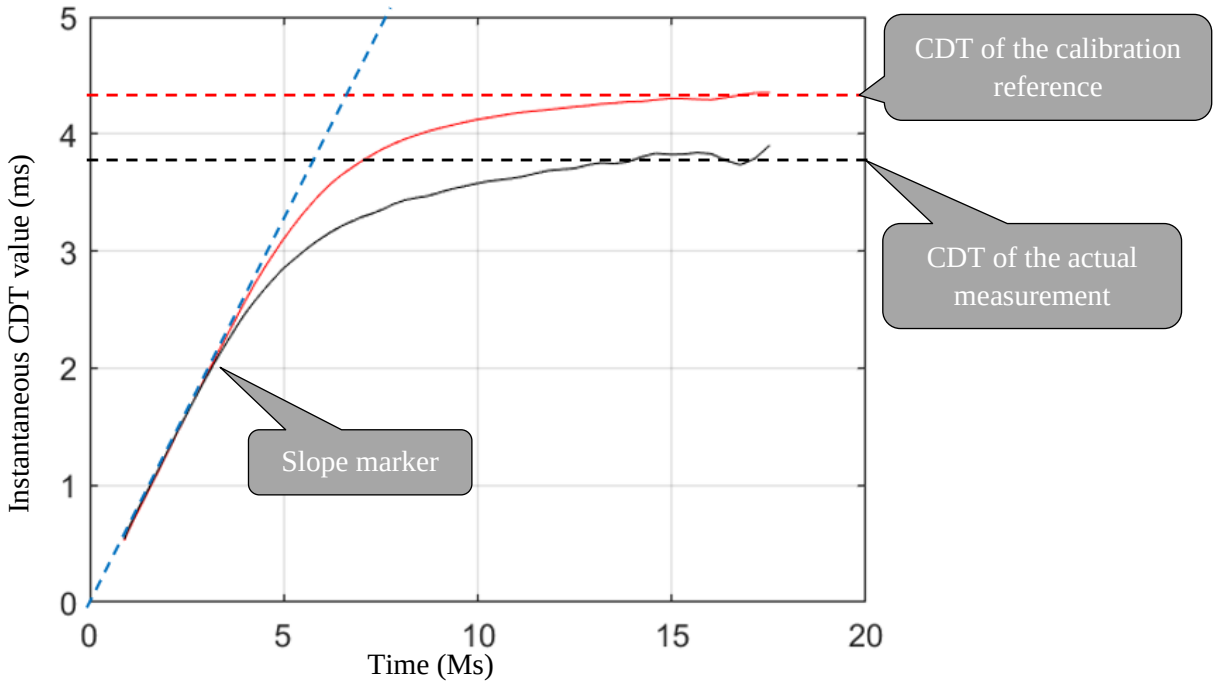

Figure 13. Essential parameters of the *Tau* curve.

3.2 Uses and applications

The most useful information that can be extracted from the *Tau* curve includes:

1. Detection of a configuration error related with weather jacket type and thickness.
2. Identify jacket overlaps potentially affecting the measurements.
3. Highlight problems with the setup.
4. Increase confidence for the detection of small defects.
5. Improve assessment of the quality of the calibration A-scan.

But in order to understand how to interpret the *Tau* curve, let's consider Figure 13 which shows the 3 distinct phases of the *Tau* curve. These can be described as follows:

1. The first phase, shown in orange, is a rising flat line in the *Tau* curve that corresponds to the portion of the A-scan that can be represented by a power law function. It contains information related with:
    a. The type of material
    b. The weather jacket type, thickness and overlaps
    c. Contributions from interfering metallic elements near or under the probe
    d. Interference from welds
    e. Problems with the component setup
2. The second phase, shown in blue, is a transition phase between phase 1 and 3. It mainly contains information on flaws that would be smaller than the averaging area.
3. And phase 3, shown in black, is the final flat line in the Tau curve which corresponds to the portion of the A-scan that can be represented by a power law function. It contains information related with:
    a. Presence of corrosion regions larger than the probe averaging area
    b. Noise and other sources of perturbation
    c. Problems with the component setup

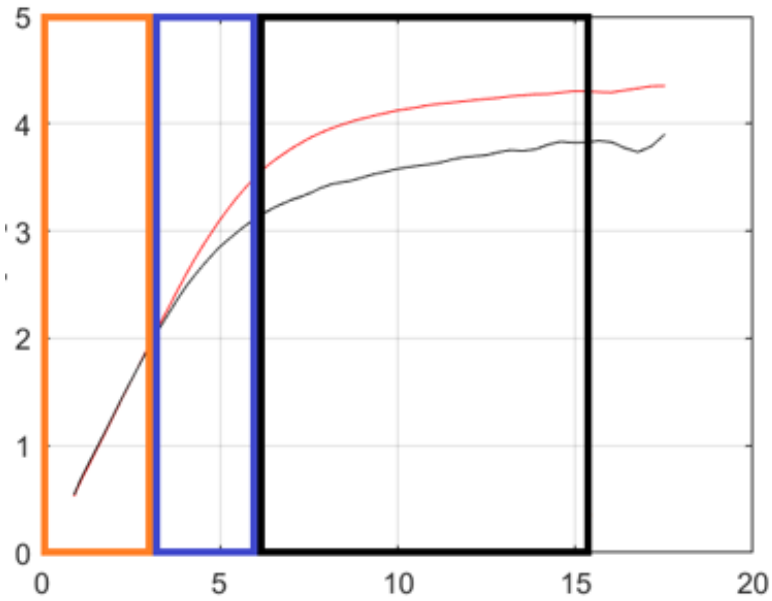

Figure 14. The three phases of a Tau curve

3.3 Application examples

Let's explore in more details a few examples of how the *Tau* curve can be used. For simplicity we'll explore only one example per phase.

3.3.1 Exploring weather jacket details in phase one of the Tau curve

One of the most useful uses of the *Tau* curve's first phase is to perform measurements related with weather jackets. It is well known that each 1 mm of aluminium induces an offset of 3 ms in the PEC signal. That offset can be clearly measured in the *Tau* curve by measuring the offset in the slope cursor. Figure 14 shows the example of a signal without aluminium in black, compared with the signal in the presence of 1 mm of aluminium in blue. The offset due to the aluminium layer is measurable using an extrapolation of the slope marker on the time axis. In this case, we measure 3 ms which concurs with theory.

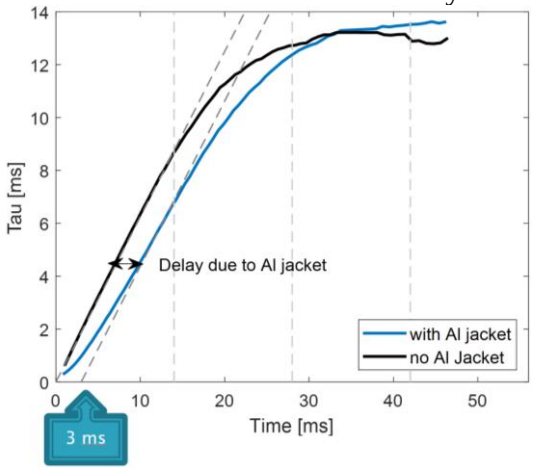

Figure 15. Using phase one of the *Tau* curve to estimate aluminum weather jacket thicknesses. In this case, the projection of the slope marker on the time axis points to 3 ms which corresponds to an aluminum layer 1 mm thick.

Based on the same concept, problems related with weather jackets such as the following can be detected:

1. Error in the weather jacket nominal thickness configuration
2. Error in the configured weather jacket material
3. Excessive jacket overlaps that would lead to errors in the measurements

3.3.2 Identify risks associated with flaw depth under sizing using phase 2 of the *Tau* curve

Phase 2 of the *Tau* curve can be used to confirm that we're in presence of a flaw which is smaller than the area over which PEC averages the wall thickness measurement. Such flaws are underestimated in depth. It is therefore relevant to confirm that one is indeed facing such a condition. Figure 15 shows the superimposed signals of a flaw larger than the averaging area in black and a flaw smaller than the averaging area in blue against the calibration reference in red. A flaw larger than the averaging area will quit the calibration reference curve late in time and will show distinctive flat lines in the first and third phase of the *Tau* curve. On the other hand, a flaw smaller than the averaging area will quit the calibration reference curve early in time and the phase 1 portion of the *Tau* curve will be slightly curvy and its slope will not follow the calibration reference slope marker.

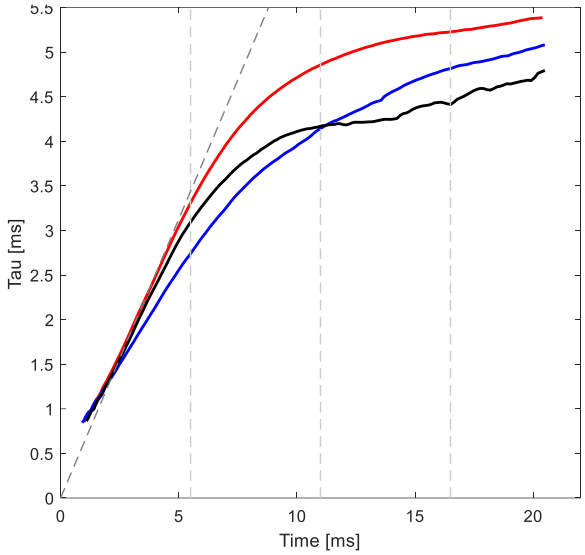

Figure 16. Comparison between a flaw which is larger than the PEC averaging area in black and a flaw smaller than the averaging area in blue.

3.3.3 Confirming effective PEC setup using phase 3 of the *Tau* curve

One of the critical aspects of a PEC setup is to obtain full penetration of the magnetic fields during the pulse phase of the PEC process, then obtain all of the meaningful information in the A-scan. The SmartPulse™ automated setup is meant to guarantee that such conditions are obtained but before the Tau curve, an inspector had no means of making sure these conditions were obtained during the automated setup. As mentioned earlier, phase 3 of the *Tau* curve can be used to detect errors in the setup that would lead to bad inspection. Figure 16 shows the example of a bad setup in which the complete penetration of the inspected component is not achieved. In the A-scan, nothing tells the inspector that something is wrong with the setup but in the *Tau* curve, it is clear that something is wrong as the phase 3 plateau is never reached.

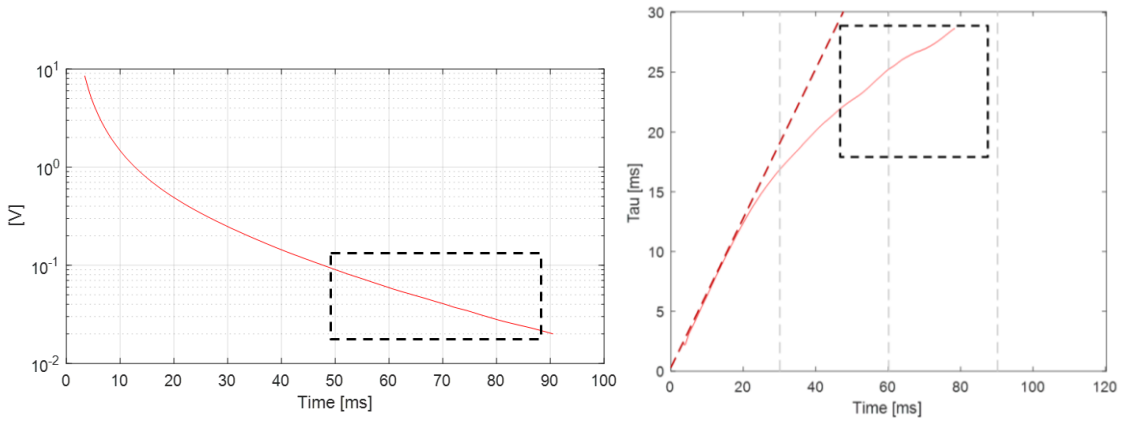

Figure 17. A bad PEC setup represented using a log-lin A-scan on the left, and the *Tau* curve on the right. Nothing wrong shown up on the A-scan but when looking at the Tau curve, the phase 3 plateau is never reached which indicates an important problem in the PEC setup

4 CONCLUSION

PEC always presented great opportunities to learn about the state of critical, but invisible parts of valuable assets, and that in the most economical way. It makes possible, for instance, the inspection of corroding deck plates on ships, without destroying the floor coverings and the inspection of corroding piping systems through thick corrosion scabs, not requiring its removal and therefore making the inspection process much safer and less destructive.

Prevalent technological limitations that hindered PEC inspections left service providers and asset owners with something better to wish for: Improving the probability of detection, minimize false calls and improve the accuracy of the measurements.

Through deep innovations, previously untackled technological obstacles were overcome. These innovations resulted in two new and unique technologies. The first one is a sensor with a much improved POD and accuracy while retaining the application range which makes it practical to the industry. The second one is a new PEC signal representation that makes possible for an analyst to clearly understand for the first time what a PEC signal tells him, which is critical to increase his confidence level in the calls he makes, indirectly promoting a better POD, and reducing false calls.

This is just another example that through technological innovations, we can hope for a cleaner, safer and healthier future.

5 REFERENCES

[1] Smith, R. A., and Hugo, G. R., 2001, “Transient Eddy-Current NDE for Aging Aircraft – Capabilities and Limita-tions,” Insight: Non-Destructive Testing and Condition Monitoring, 43(1), pp. 14–25.

[2] Moulder, J. C., Kubovich, M. W., Uzal, E., and Rose, J. H., 1995, “Pulsed Eddy-Current Measurements of Corrosion-Induced Metal Loss: Theory and Experiment,” Review of Progress in Quantitative Nondestructive Evaluation, Spring-er, Boston, MA, pp. 2065–2072.

[3] Demers-Carpentier, V., Rochette, M., Grenier, M., Trem-blay, C., Sisto, M. M., Hardy, F., and Turgeon, M., 2016, “Pulsed Eddy Current as an Inspection Tool for Nuclear Power Plants,” NDT in Canada 2016 & 6th International CANDU In-Service Inspection Workshop, Burlington, ON.

[4] Grenier, M., Demers-Carpentier, V., Rochette, M., and Har-dy, F., 2016, "Pulsed Eddy Current: New Developments for Corrosion Under Insulation Examinations," Munich, Ger-many.
[5] Cheng, W., 2012, "Pulsed Eddy Current Testing of Carbon Steel Pipes' Wall-Thinning through Insulation and Clad-ding," Journal of Nondestructive evaluation, 31(3), pp. 215–224.
[6] Crouzen, P., and Munns, I., 2006, "Pulsed Eddy Current Corrosion Monitoring in Refineries and Oil Production Facilities–experience at Shell," signal, 2(3), p. 4.